DENTAL MATERIALS 35 (2019) 697–708

Available online at www.sciencedirect.com

ScienceDirect

journal homepage: www.intl.elsevierhealth.com/journals/dema

Microstructural development during heat treatment of a commercially available dental-grade lithium disilicate glass-ceramic

Angel L. Ortiz[a,*], *Oscar Borrero-López*[a], *Fernando Guiberteau*[a], *Yu Zhang*[b]

[a] *Departamento de Ingeniería Mecánica, Energética y de los Materiales, Universidad de Extremadura, 06006 Badajoz, Spain*

[b] *Department of Biomaterials and Biomimetics, New York University College of Dentistry, NY 10010, USA*

ARTICLE INFO

Article history:
Received 13 September 2018
Received in revised form
21 January 2019
Accepted 7 February 2019

Keywords:
Lithium disilicate
Dental materials
Glass-ceramics
Microstructural evolution
In-situ characterizations

ABSTRACT

Objective. To elucidate the microstructural evolution of a commercial dental-grade lithium disilicate glass-ceramic using a wide battery of in-situ and ex-situ characterization techniques.

Methods. In-situ X-ray thermo-diffractometry experiments were conducted on a commercially available dental-grade lithium disilicate glass-ceramic under both non-isothermal and isothermal heat treatments in air. These analyses were complemented by experiments of ex-situ X-ray diffractometry, field-emission scanning electron microscopy, energy-dispersive X-ray spectroscopy, differential scanning calorimetry, and field-emission scanning electron thermo-microscopy.

Results. It was found that the non-fired blue block consists of ~40 vol% crystals embedded in a glass matrix. The crystals are mainly lithium metasilicate (Li_2SiO_3) along with small amounts of lithium orthophosphate (Li_3PO_4) and lithium disilicate ($Li_2Si_2O_5$). Upon heating, the glassy matrix in the as-received block first crystallizes partially as SiO_2 (i.e., cristobalite) at ~660 °C. Then, the SiO_2 crystals react with the original Li_2SiO_3 crystals at ~735 °C, forming the desired $Li_2Si_2O_5$ crystals by a solid-state reaction in equimolar concentration ($SiO_2 + Li_2SiO_3 \rightarrow Li_2Si_2O_5$). Precipitation of added colourant Ce ions in the form of CeO_2 appears at ~775 °C. These events result in a glass-ceramic material with the aesthetic quality and mechanical integrity required for dental restorations. It also has a microstructure consisting essentially of elongated $Li_2Si_2O_5$ grains in a glassy matrix plus small cubic CeO_2 grains at the outermost part of the surface.

Significance. It was found that by judiciously controlling the heat treatment parameters, it is possible to tailor the microstructure of the resulting glass-ceramics and thus optimizing their performance and lifespan as dental restorations.

* Corresponding author.
E-mail address: alortiz@unex.es (A.L. Ortiz).

https://doi.org/10.1016/j.dental.2019.02.011

1. Introduction

Lithium disilicate glass-ceramic was first introduced to dentistry by Beall & Echeverria [1], and commercialized by Ivoclar Vivadent in 1998 with the trade name IPS Empress 2. This material was fabricated using the lost-wax press technique, and was indicated for single-unit crowns and anterior 3-unit fixed dental prostheses (FDPs) [2–4]. Medium-term clinical studies showed that, while the survival rates for single-unit crowns were satisfactory, those for FDPs were poor, being 87% at 4 yr [5], 70% at 5 yr [2], and 63% at 6 yr [6].

In an effort to improve the mechanical and optical properties of Empress 2, two new lithium disilicate based glass-ceramic materials, namely IPS e.max Press and CAD, have been developed [7–10]. The improvements in the IPS e.max system were achieved through the refinement of the base glass composition as well as the quality of the starting glass ingots. The base glass composition for e.max has substituted the La_2O_3 additives in Empress 2 with approximately 4 wt % ZrO_2 [11]. The starting ingots of e.max have also possessed fewer defects (pores, accumulation of pigments, etc.) relative to Empress 2 [11].

The IPS e.max materials can be fabricated using either the traditional press technique or CAD/CAM technology. The high crystal density (up to ~70 vol.%) of these glass-ceramic materials after firing ensures both high strength (460–500 MPa) and high toughness (2.1–2.5 MPa $m^{1/2}$), while maintaining outstanding aesthetic properties [12,13]. Clinical studies reveal that IPS e.max prostheses exhibited much improved survival rates relative to their Empress 2 counterparts [14,15]. However, despite the major clinical successes of the IPS e.max system, a fundamental understanding of its microstructural development is still lacking [16].

IPS e.max Press was released in 2001. A few years later, IPS e.max CAD was developed to improve the efficiency of prosthesis fabrication [17]. In the latter case, the fabrication process begins with a prefabricated partially crystallized glass-ceramic block, which is relatively soft but strong enough for machining and edge stability. After milling, the restorations are then crystallized to form a lithium disilicate glass-ceramic material via a thermal treatment. Such a thermal treatment involves a nucleation and crystallization process, which, in turn, controls the mechanical and optical properties of the final glass-ceramic [18,19]. Thus, to optimize the properties of the glass-ceramic, a comprehensive understanding of the nucleation and crystallization process is paramount. To date, most studies on nucleation and crystallization kinetics were conducted using ex-situ characterization techniques at room temperature, meaning that the specimens were fabricated and cooled down to room temperature for phase analysis and microstructural examination [16,18–24]. If not done properly, the phase assembly and microstructure can change during cooling. In addition, it is extremely challenging to understand the entire microstructural evolution relying solely on ex-situ characterization techniques. There have been only a few in-situ studies, but most used custom-designed glass compositions and heat treatment routes which differ from the commercial glass composition and heating ramp [20–30].

With these premises in mind, in the present study we systematically examined the microstructural development of a renowned, commercially available, lithium disilicate dental glass-ceramic using a wide battery of both in-situ and ex-situ techniques. Specifically, we selected the world's best-selling glass-ceramic material (IPS e.max CAD) [31], and exhaustively characterized it under various heat treatment conditions including the one recommended by the manufacturer and routinely adopted in dental laboratories. Finally, clinical implications of the findings are discussed.

2. Experimental procedure

The starting material was a commercially available dental-grade lithium disilicate block (IPS e.max CAD HT, C14, Shade A2; Ivoclar Vivadent, NY). According to the manufacturer, the as-received block is a partially crystallized glass-ceramic of blue colour (therefore referred to as the "blue block"). It is prepared by the controlled crystallization of glass ingots whose standard composition (in wt %) is 57–80 SiO_2, 11–19 Li_2O, 0–13 K_2O, 0–11 P_2O_5, 0–8 ZrO_2, 0–8 ZnO, 0–5 Al_2O_3, 0–5 MgO, and 0–8 colouring oxides. IPS e.max CAD was used because it is the best-selling glass-ceramic material in the world [31]. The HT grade was selected because the chemical composition of the lithium disilicate crystals and its glass matrix is most similar in comparison to its MO or LT counterparts. Slides (~1 mm thickness) were cut from the as-received block, which were next machined into parallelepiped plates (~$14 \times 12 \times 1\ mm^3$) and diamond polished to a 1-μm finish for their use in the present study. The microstructural development of this blue block during its heat treatment was then examined using a slew of both in-situ and ex-situ characterization techniques, as described below.

First of all, the blue block was characterized in detail. Specifically, its crystallization state was investigated by X-ray diffractometry (XRD; D8 Advance, Bruker AXS, Germany) using a high-resolution diffractometer equipped with a linear ultra-fast detector. The XRD pattern was collected over the angular range 10–60° 2θ using CuKα_1 incident radiation ($\lambda = 1.5406$ Å) and a step size and counting time of 0.016° 2θ and 3 s, respectively. The crystalline phases present were identified using the PDF2 database integrated in the evaluation package Diffrac^{plus} (Diffrac^{plus} Basic, EVA, Bruker AXS, Germany). The microstructure was examined by field-emission scanning electron microscopy (FE-SEM; Quanta 3D FEG, FEI, The Netherlands) using unetched specimens. Imaging was performed on uncoated specimens at random locations, operating at 20 keV in low-vacuum mode (at 80 Pa pressure) with the (gaseous analytical) backscattered electron detector (BSED). The degree of crystallinity (defined as the fraction of crystallized area) and the morphology of the crystals (length and thickness) were calculated from the SEM images by image analysis (AnalySIS, Olympus Soft Imaging Solutions GmbH, Germany). In addition, the elemental chemical composition (at.%) was measured by energy-dispersive X-ray spectroscopy (EDXS), using the ZAF-factor technique for the quantitative analyses. The EDXS spectra were taken in the energy range 0.1–10 keV at random locations, again operating at 20 keV.

The microstructural evolution of the blue block was subsequently investigated, during both non-isothermal and isothermal heat treatments in air. In particular, its crystallization was investigated in-situ by X-ray thermo-diffractometry (XRTD), using the same diffractometer as before but equipped with a furnace-type heating chamber (as done before in other ceramics [32–36]). More specifically, the chamber (RP-Furnace, MRI, Germany) consists essentially of a tube-like heater made of Pt-Rh with proper thermal insulation, where an Al_2O_3 holder with the sample is inserted. The temperature is measured with a type-S thermocouple located at the sample surface, and the heating is regulated by a power unit integrated with a PID-controller. Note that for accurate in-situ XRTD studies on these materials, it is necessary to use this heating chamber geometry instead of the more typical strip-heater type heating stages used in earlier work [23,28–30], in which the specimens are simply heated on a hot filament from the lower surface despite the XRTD data are collected from the top surface. Since most glass-ceramics and ceramics have poor thermal conductivity, the use of a hot-strip type heating stage is likely to lead to large differences between the set temperature of the hot filament and the actual temperature at the specimen surface. The furnace-type heating chamber ensures accurate temperatures and the optimal thermal uniformity of the measurable surface [32], and in addition imitates the radiative heating of the furnaces available for dental laboratories.

Three sets of XRTD patterns were collected over the angular range 15–45° 2θ with step size of 0.016° 2θ and counting time of 0.1 s, and delay time of 2 s for temperature stabilization. Firstly, they were measured under non-isothermal heating conditions each 5 °C in the temperature range 30–900 °C (using an effective heating ramp of ~0.9 °C/min). This first in-situ XRTD study was aimed at gaining detailed insights into the occurrence of sequential events (such as reactions, crystallizations, precipitations, etc.). Secondly, they were measured under an isothermal heating regime at 770 °C (reached using a heating ramp of 60 °C/min) with 2 °C fluctuation, each 2 min in the holding time ranging from 0–60 min. And thirdly, they were measured under an isothermal heating regime at 850 °C (reached using a heating ramp of 60 °C/min up to 770 °C and there onwards at 30 °C/min) with 2 °C fluctuation, each 2 min in the holding-time range 0–60 min. The design of these second and third in-situ XRTD studies was to follow the manufacturer's recommendation as implemented by dental laboratories, which proposes a crystallization cycle with a heating ramp of 60 °C/min up to 770 °C and holding there for 10 s followed by a second heating ramp of 30 °C/min up to 850 °C and holding there for 10 min. Nonetheless, in the present in-situ XRTD studies the holding times were varied intentionally in the range of 0–60 min to investigate their effect on the microstructural development. XRD patterns were also collected once the specimen had cooled down naturally to room temperature. In addition, the surface microstructure of the resulting blocks was characterized by FE-SEM under the same conditions as before, using both the low-vacuum secondary electron detector (LVSED) and the BSED, and EDXS.

The microstructure of the blocks subjected to non-isothermal heat treatment up to 900 °C was selectively investigated in more detail. Specifically, a cross-section (25 μm length, and 8 μm depth) was prepared from its central region by in-situ lift-out techniques using a focused ion beam (FIB; Quanta 3D FEG, FEI, The Netherlands), which was then characterized by FE-SEM (with the BSED) coupled with EDXS. This block was also intentionally broken, and its fracture surface was examined by FE-SEM (with the BSED).

The XRTD studies performed on the blue block were complemented by differential scanning calorimetry (DSC; STA 449 F3 Jupiter, Netzsch, Germany) and field-emission scanning electron thermo-microscopy (FE-SETM). The DSC curves were registered in flowing pure air (at 50 ml/min) in the temperature range 30–900 °C, using heating ramps of either 1.2 (close but faster than that used in the non-isothermal XRTD study) or 10 °C/min (typically adopted in many DSC studies). This was done because slower heating rates provide better temperature resolution, while faster heating rates increase the sensibility of the heat flow measurements. The FE-SETM observations were conducted using the same field-emission gun microscope as before, but equipped with a hot-stage (heating stage module with a type-K thermocouple, and power unit with a PID-controller) and operated at 20 keV in environmental mode (at 90 Pa pressure) with the (gaseous) secondary electron detector (GSED). High-temperature in-situ imaging was done at 750, 800, and 900 °C (achieved with a heating ramp of 15 °C/min), after 5 min of soaking for temperature stabilization. The choice of these temperatures is based on the manufacturer's recommendation of using firing cycles above 750 °C; the heating ramp was, however, slower than the manufacturer's recommendation to ensure that the hot-stage provides a homogeneous surface heating.

3. Results and discussion

Fig. 1 shows a representative FE-SEM image of the blue block. It has the typical microstructure of glass-ceramics, with ceramic crystals embedded in a glassy matrix. The crystals account for ~40 vol % (crystallinity degree), and have a rod-like shape

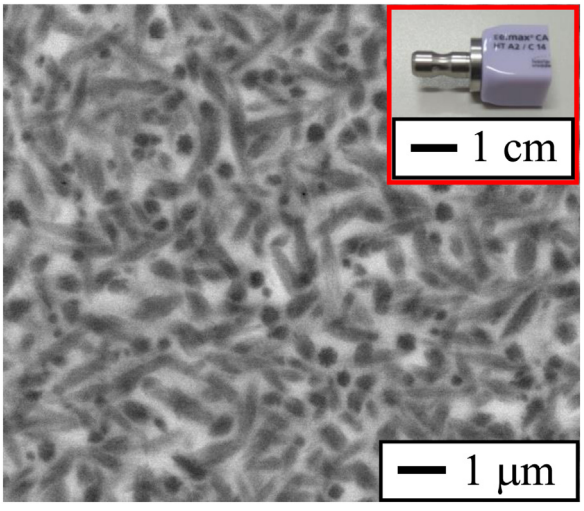

Fig. 1 – Representative SEM micrograph of the blue block in its as-received condition. The inset is an optical photograph of the blue block (from which slices were cut for the characterization studies).

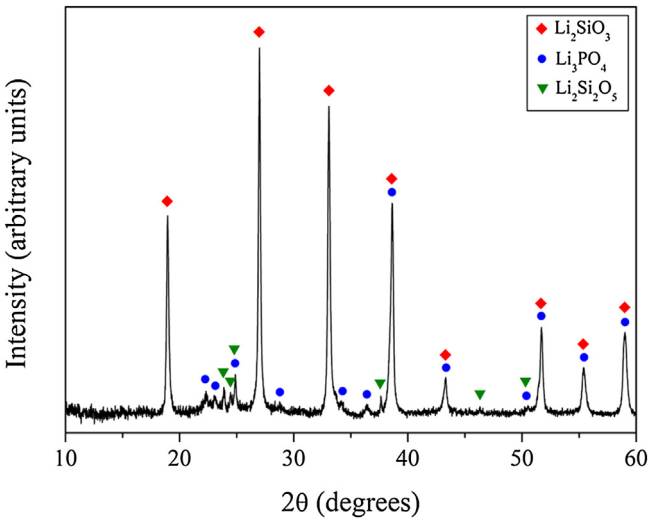

Fig. 2 – XRD pattern of the blue block. Peak assignations are included.

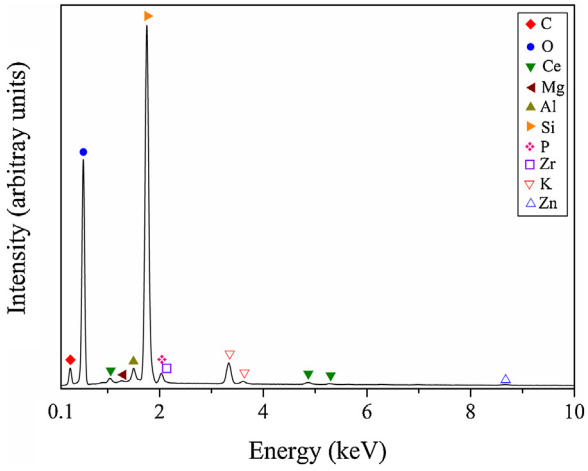

Fig. 3 – EDXS spectrum (taken in area mode) of the blue block. Peak assignations are included.

with lengths and thicknesses of ~0.5–1.5 and ~0.2–0.5 μm, respectively. According to the XRD pattern shown in Fig. 2, the crystals are mostly Li_2SiO_3 (lithium metasilicate), although a few are Li_3PO_4 (lithium orthophosphate) and $Li_2Si_2O_5$ (lithium disilicate). The weak broad hump in the XRD pattern (~20–30° 2θ) indicates the presence of a glassy phase as well, which is a SiO_2-based glass given the chemical composition of the glass ingots used to prepare the blue block. As seen in the EDXS spectrum shown in Fig. 3, this glass-ceramic also contains Ce (0.24 at.%), Al (1.05 at.%), Mg (0.10 at.%), Zr (0.28 at.%), K (1.97 at.%), and Zn (0.24 at.%), which must all be dissolved in the glassy matrix (i.e., incorporated into the glass structure as either network modifiers or intermediates). This latter is because the position of the diffraction peaks of Li_2SiO_3, Li_3PO_4, and $Li_2Si_2O_5$ matches the theoretical expectations, which rules out the formation of crystalline solid solutions.

Fig. 4 shows the three-dimensional plot of the XRTD patterns collected in-situ during the non-isothermal heating of the blue block from 30 to 900 °C in air. It can be seen that its partially crystalline state does not change up to ~660 °C, at which temperature a transient crystalline phase precipitates from the glass. Both these transient crystals and the Li_2SiO_3 crystals disappear completely at ~760 °C, giving rise to a new permanent crystalline phase. Finally, another permanent crystalline phase appears at ~775 °C. Fig. 5 shows the two-dimensional contour plot generated from the XRTD patterns in Fig. 4, together with the corresponding phase identification. With increasing temperature up to ~660 °C, the inventory of crystalline phases remains unchanged with respect to room temperature. The only phenomenon occurring in this temperature interval is the thermal expansion of the unit cells of Li_2SiO_3, Li_3PO_4, and $Li_2Si_2O_5$, as deduced from the peak shifting towards lower diffraction angles. At ~660 °C, SiO_2 crystallizes as cristobalite from the glass, as inferred from the appearance of the corresponding diffraction peaks and the substantial reduction in the background level. This cristobalite is, however, a transient crystalline phase that disappears completely at ~760 °C, which also happens for Li_2SiO_3. $Li_2Si_2O_5$ is formed concurrently with the progressive disappearance of SiO_2 and Li_2SiO_3 in the temperature interval ~735–760 °C, indicating that the gradual occurrence of the solid-state reaction $Li_2SiO_3+SiO_2 \rightarrow Li_2Si_2O_5$. Once formed, $Li_2Si_2O_5$ is a permanent crystalline phase. Finally, at ~775 °C CeO_2 appears, a phenomenon that is nonetheless much more evident at ~835 °C. The CeO_2 crystals exhibit preferred orientation along their <100> directions (i.e., the cube faces) because the 200 diffraction peak (at ~32.8° 2θ) is, contrary to the theoretical expectation, stronger than the 111 diffraction peak

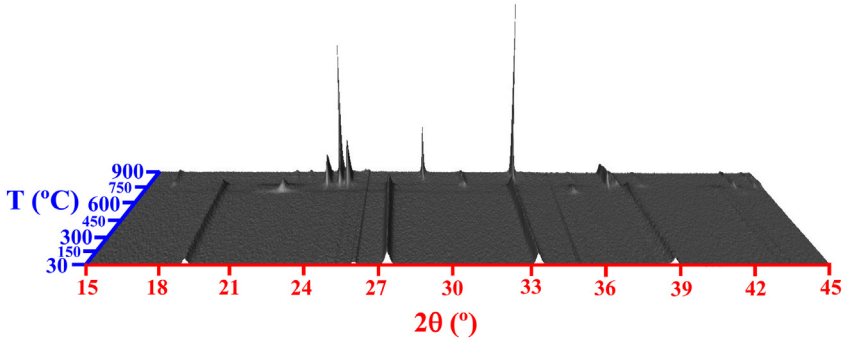

Fig. 4 – XRTD patterns (angular interval 15–45° 2θ) collected in-situ as a function of the temperature (T) in the range 30–900 °C for the blue block.

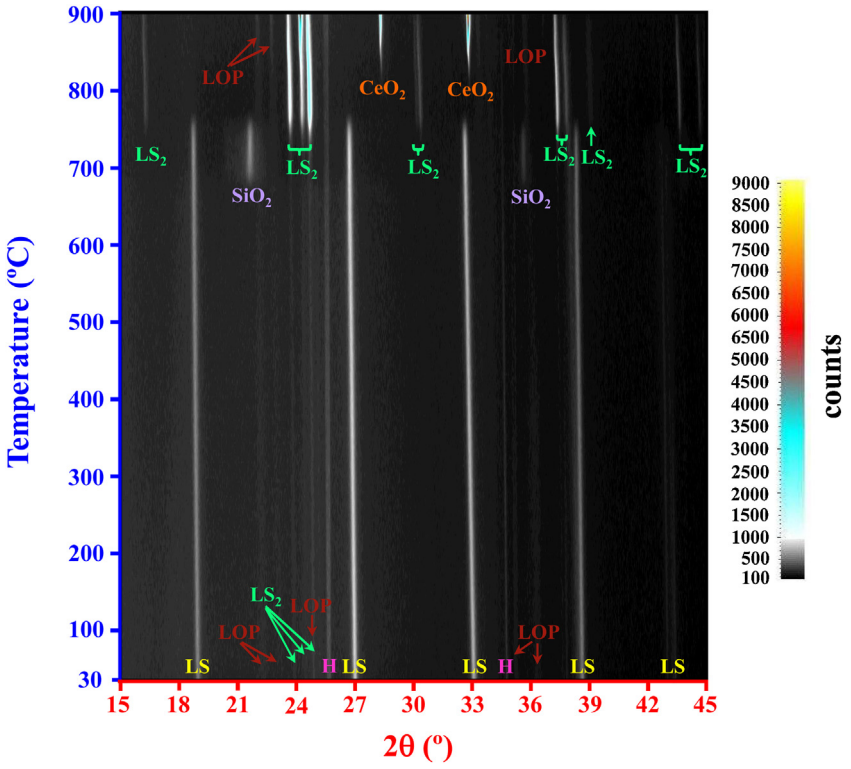

Fig. 5 – Two-dimensional intensity contour (extracted from the XRTD patterns) as a function of the temperature in the range 30–900 °C for the blue block. Line assignations are included (LS = Li_2SiO_3, LS_2=$Li_2Si_2O_5$, LOP = Li_3PO_4, and H = Al_2O_3 holder).

(at ~28.3° 2θ). Also, CeO_2 appearance comes accompanied by a sudden decrease in the lattice parameters of $Li_2Si_2O_5$, as inferred from the slower temperature dependence of the peak shifting. It is then reasonable to presume that CeO_2 precipitated, at least partially, from $Li_2Si_2O_5$, and, consequently, that Ce was necessarily dissolved in solid solution within the $Li_2Si_2O_5$ host. In particular, Ce would have substituted partially for Si thus forming $Li_2Si_{2-x}Ce_xO_5$ without oxygen vacancies, which has larger lattice parameters than $Li_2Si_2O_5$ due to the larger cationic size (by a factor of 2) of Ce^{4+} relative to Si^{4+}. The phenomenon of CeO_2 precipitation observed here is quite novel, and to the best of the authors knowledge has

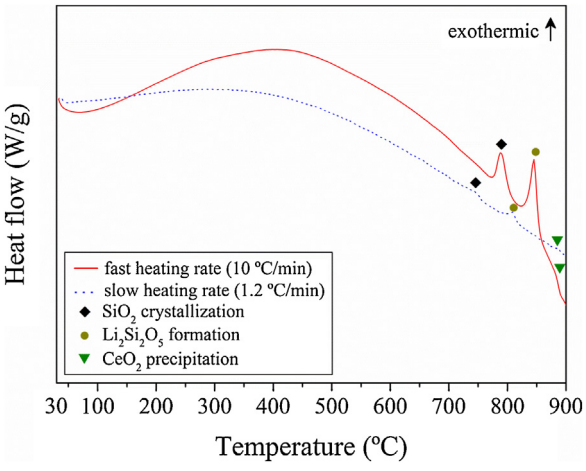

Fig. 6 – DSC curves measured as a function of the temperature in the range 30–900 °C for the blue block. The heating ramps used are indicated. Peak assignations are included.

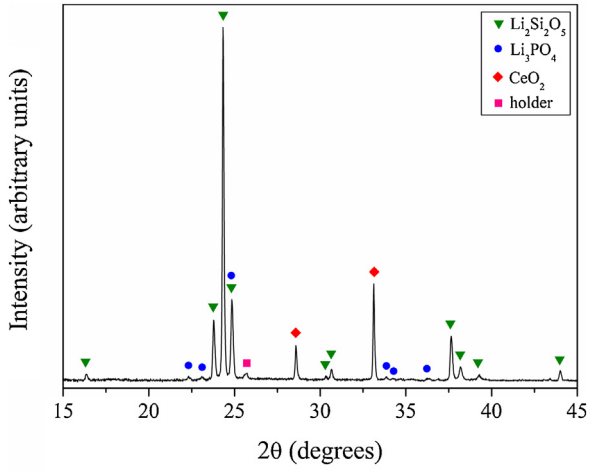

Fig. 7 – XRD pattern of the block resulting from the non-isothermal heating up to 900 °C. Peak assignations are included.

not been reported before. Nonetheless, careful re-evaluation of earlier in-situ XRTD studies performed on other custom-designed glass compositions also indicates CeO_2 precipitation [27], therefore demonstrating that it is not exclusive to the present commercially available glass-ceramic. CeO_2 precipitation could also have gone unnoticed in earlier studies if, as it is common practice, the specimens are polished and/or etched with acids prior to their microstructural characterization.

It is also worth mentioning at this point that the evolution on the temperature of the lithium disilicate based glasses and glass-ceramics is both qualitatively and quantitatively affected by factors such as their composition, thermal history, and heat treatment condition, which reinforces the need for a study such as the present on the commercially available material. Thus, for example, unlike what happens with other custom-designed glass compositions [23], the precipitation of ZrO_2 or of other oxides (Al_2O_3, MgO, ZnO, etc.) was not observed here, suggesting that these ions remain in the glass matrix. Crystallization of the SiO_2 matrix as cristobalite has been observed for the present glass-ceramic, but not for other similar glasses [23]. Matrix crystallization as both cristobalite and quartz has been reported as well [23,25,30], not only as cristobalite. Lastly, the onset temperatures of the different events occurring are not always the same, but may differ appreciably [37].

Fig. 6 shows the DSC curves of the blue block registered from ~30 to 900 °C in air. They exhibit the peaks attributable to SiO_2 crystallization, $Li_2Si_2O_5$ formation, and CeO_2 precipitation already observed by XRTD. The temperatures registered for these events are, however, slightly higher in DSC than in XRTD, but this can simply be due to the combination of various factors such as the faster heating rates used in the former (confirmed here by using two different heating rates during DSC), the different heating protocols applied (stepwise heat-

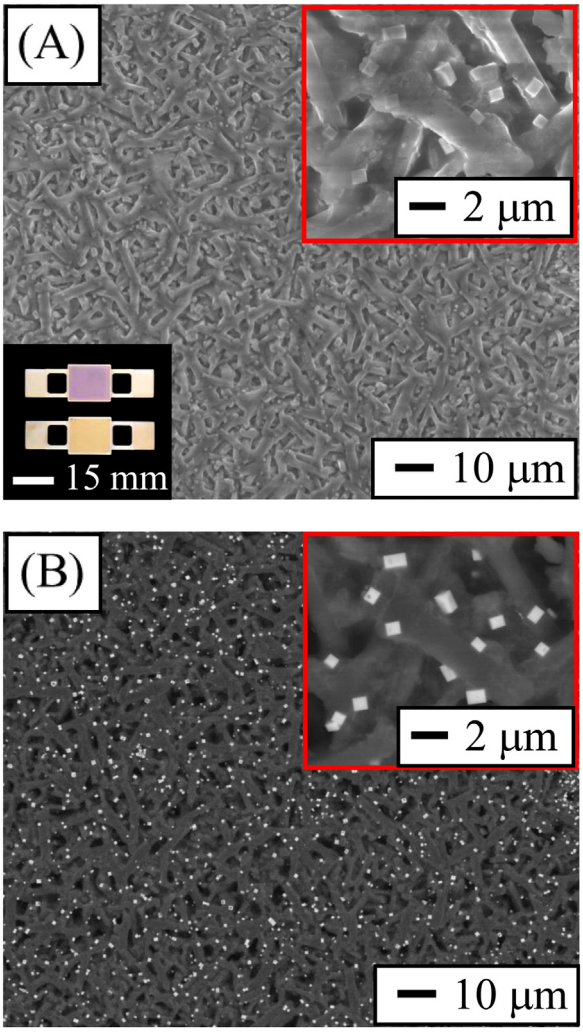

Fig. 8 – Representative SEM micrographs of the block resulting from the non-isothermal heating up to 900 °C, taken with the (A) LVSED and (B) BSED. The insets in (A) and (B) are higher-magnification micrographs. The other inset in (A) shows blue block and the block non-isothermally heat-treated up to 900 °C.

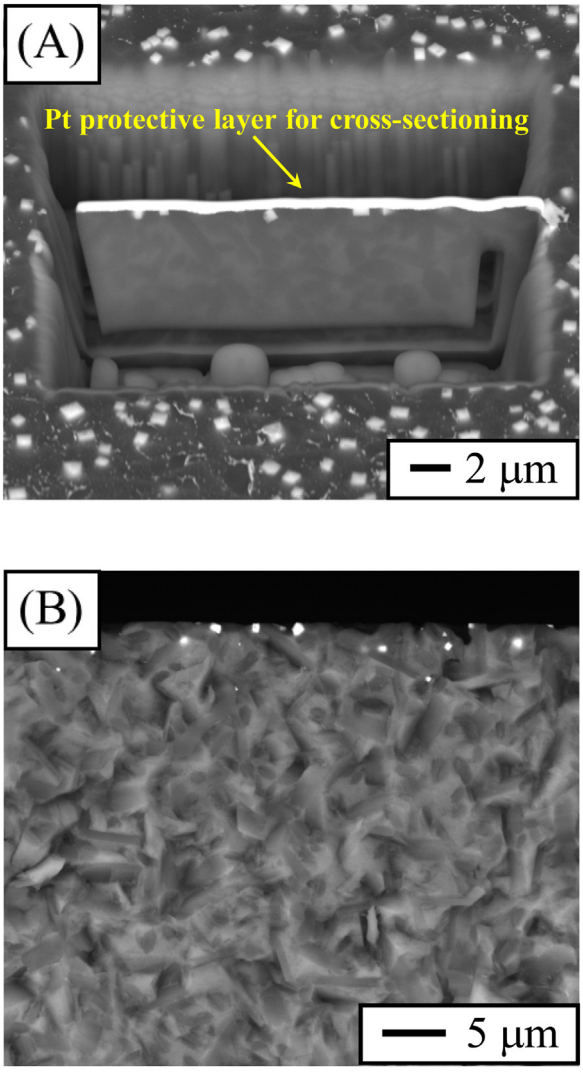

Fig. 9 – Representative SEM micrographs taken with the BSED (A) of the cross-section prepared by in-situ lift-out in the FIB microscope, and (B) of the fracture surface (broken intentionally) of the block non-isothermally heat-treated up to 900 °C.

ing in XRTD to collect patterns in-situ but continuous heating in DSC), and the different atmospheres used (ambient air in XRTD but flowing pure air in DSC).

Fig. 7 shows the XRD pattern of the glass-ceramic block extracted from the diffractometer after the non-isothermal XRTD up to 900 °C. Only diffraction peaks from $Li_2Si_2O_5$ (major phase), Li_3PO_4 (minor phase), and CeO_2 (minor phase) are observed, therefore indicating that the crystalline phases formed at 900 °C do not reversibly transform during the natural cooling to room temperature. Additionally, it was confirmed that the CeO_2 crystals have crystallographic texture along their <100> directions because the intensity ratio of the 111 diffraction peak to the 200 diffraction peak is 0.27, not 2.75 as expected for randomly oriented CeO_2 crystals. Fig. 8 shows representative FE-SEM images (both LVSED and BSED images) of the surface of the resulting block, which is no longer blue but has a tooth colour with shades and translucency satisfying the aesthetic requirements needed for restorative dentistry. In addition, its microstructure is very different from that of the blue block. Firstly, there is a network of interconnected large $Li_2Si_2O_5$ crystals with glassy phase in-between instead of well-dispersed small Li_2SiO_3 crystals embedded in a glassy matrix. The $Li_2Si_2O_5$ crystals have a rod-like morphology, but their lengths and thicknesses are as great as ~20 and 3 μm, respectively. The higher aspect ratio of these $Li_2Si_2O_5$ crystals in relation to the original Li_2SiO_3 crystals indicates the occurrence of preferential crystal growth. In addition, the $Li_2Si_2O_5$ crystals now account for ~70–80 vol %, not just 40 vol %. And secondly, there are also well-faceted cubic crystals of ~1–1.5 μm in size homogeneously dispersed, identified as being CeO_2 crystals according to the BSED images and additional EDXS spectra taken in point mode (not shown). These CeO_2 crystals are mostly oriented with the cube faces parallel to the specimen surface, thus confirming the crystallographic texture already deduced by XRTD and XRD. Furthermore, microstructural observations by FE-SEM of cross-sections prepared by in-situ lift-out in the FIB microscope and of fracture surfaces (broken intentionally), such as the ones shown in Fig. 9, reveal that there are CeO_2 crystals only at the outermost part of the surface (first 1–3 μm in depth). CeO_2 is then, overall, a very minor crystalline phase, which explains the weakness of the peak attributable to CeO_2 precipitation in the DSC curves. Also, the absence of CeO_2 crystals in the interior of the heat-treated block suggests that the surrounding air atmosphere plays a fundamental role in their formation.

For clinical practice, the manufacturer recommends for dental prosthetics that the dental piece machined from the blue block be subjected to a two-stage heat treatment. The recommended firing cycle consists of a first heating ramp at ~60 °C/min up to ~770 °C and soaking there for ~10 s, followed by a second heating ramp at ~30 °C/min up to ~850 °C and soaking there for ~10 min. Nonetheless, longer heat treatments at these, or at very close, temperatures have also been applied to this type of dental glass-ceramics. Consequently, it was considered worth examining the effect of the heat treatment duration at both 770 and 850 °C (reached

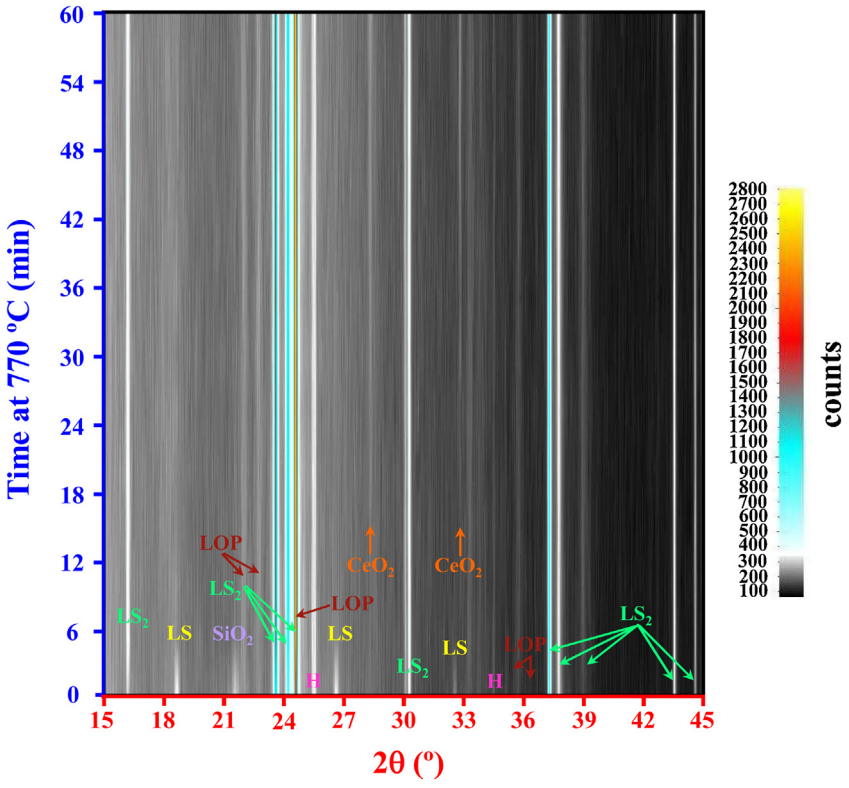

Fig. 10 – Two-dimensional intensity contour (extracted from the XRTD patterns) as a function of the holding time at 770 °C in the range 0–60 min for the blue block. Line assignations are included (LS = Li_2SiO_3, LS_2 = $Li_2Si_2O_5$, LOP = Li_3PO_4, and H = Al_2O_3 holder).

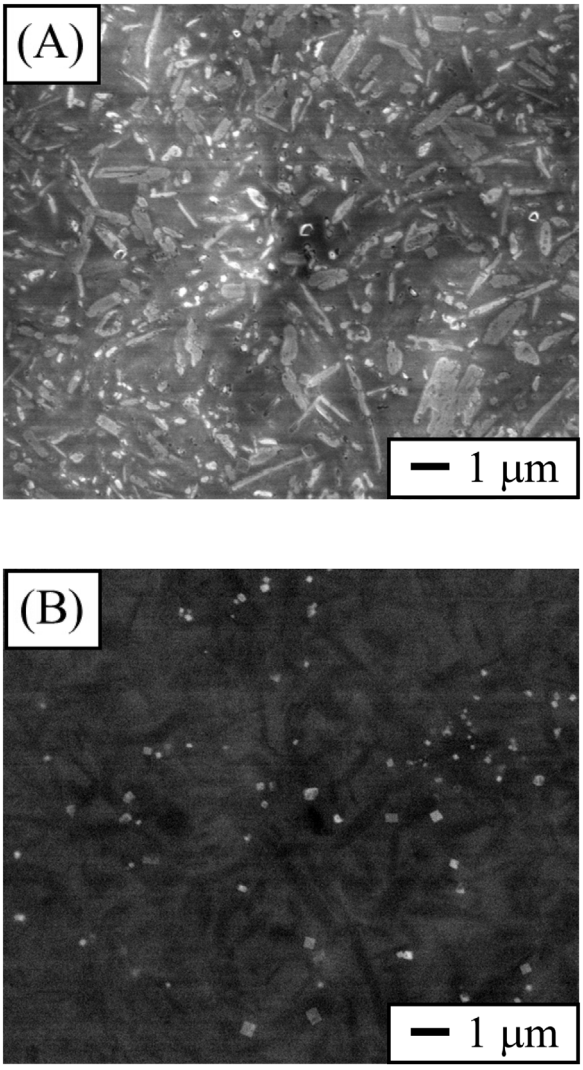

Fig. 11 – Representative SEM micrographs of the block resulting from the isothermal heating at 770 °C for 1 h, taken with the (A) LVSED and (B) BSED.

using the heating ramps proposed by the manufacturer) on the microstructural development of this commercially available dental-grade lithium disilicate glass-ceramic, as will be described in the following two paragraphs.

Fig. 10 shows the two-dimensional contour plot generated from the XRTD patterns (not shown) collected in-situ during the isothermal heating of the blue block at 770 °C as a function of time up to 1 h, together with the corresponding phase identification. As expected, at 770 °C there are initially $Li_2Si_2O_5$ (major phase) and Li_3PO_4 (minor phase) crystals, and still some unconsumed Li_2SiO_3 and SiO_2 (i.e., cristobalite) crystals. This is because the kinetics of the solid-state reaction $Li_2SiO_3+SiO_2 \rightarrow Li_2Si_2O_5$ is slower during the isothermal heating (due to the faster heating ramp). The reaction is however completed after ~6 min at 770 °C. Finally, after ~15 min at 770 °C there is a marginal CeO_2 precipitation. Fig. 11 shows representative FE-SEM images (both LVSED and BSED images) of the surface of the resulting block, which also turned tooth colour (not shown). Its microstructure consists essentially of $Li_2Si_2O_5$ crystals embedded in a glassy matrix, plus sparse CeO_2 cubic crystals (with crystallographic texture). The $Li_2Si_2O_5$ crystals are relatively fine (lengths and thicknesses less than 2 and 0.8 μm, respectively), and have a rod-like shape. Therefore, this microstructure differs substantially from that of the block non-isothermally heat-treated up at 900 °C, but bears a certain resemblance to that of the blue block (albeit with $Li_2Si_2O_5$ crystals instead of Li_2SiO_3 crystals, higher crystallinity degree, and surface CeO_2 crystals).

Fig. 12 shows the two-dimensional contour plot generated from the XRTD patterns (not shown) collected in-situ during the isothermal heating of blue block at 850 °C as a function of time up to 1 h, together with the corresponding phase identification. From the beginning there are $Li_2Si_2O_5$ (major phase), Li_3PO_4 (minor phase), and CeO_2 (minor phase) crystals, with the abundance of surface CeO_2 increasing with the exposure

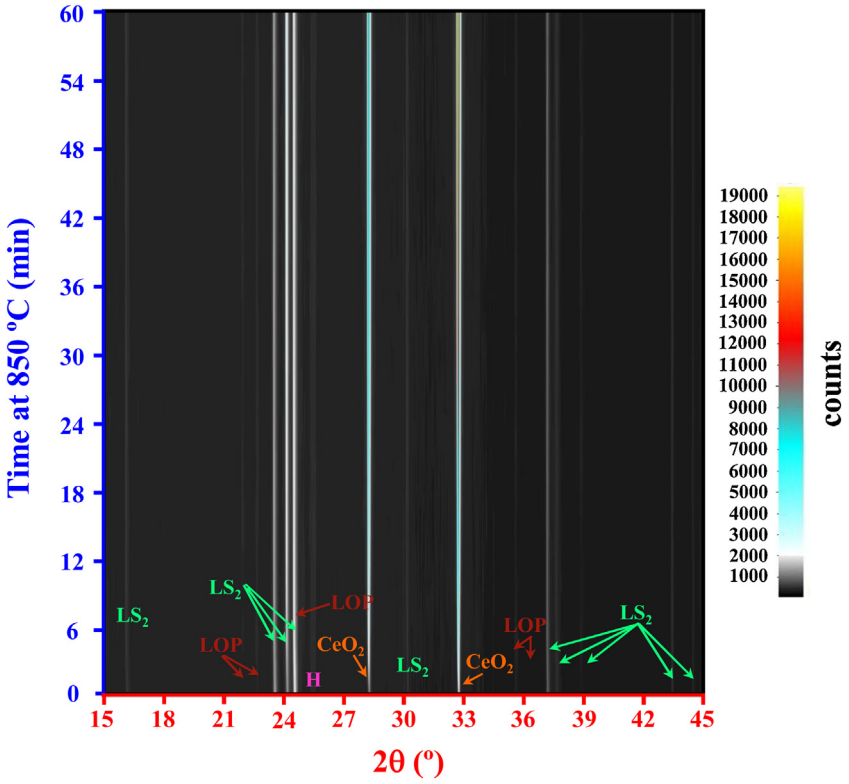

Fig. 12 – Two-dimensional intensity contour (extracted from the XRTD patterns) as a function of the holding time at 850 °C in the range 0–60 min for the blue block. Line assignations are included ($LS_2 = Li_2Si_2O_5$, LOP = Li_3PO_4, and H = Al_2O_3 holder).

time at 850 °C. Neither Li_2SiO_3 nor SiO_2 are observed, which is because the solid-state reaction $Li_2SiO_3 + SiO_2 \rightarrow Li_2Si_2O_5$ was completed at lower temperatures during the heating ramp. Fig. 13 shows representative FE-SEM images (both LVSED and BSED images) of the surface of the resulting block. Its microstructure consists essentially of $Li_2Si_2O_5$ crystals embedded in a glassy matrix, plus abundant CeO_2 cubic crystals (with preferred orientation) everywhere. The $Li_2Si_2O_5$ crystals are coarser (lengths and thicknesses less than 5 and 2 μm, respectively), and have a rod-like shape. Therefore, this microstructure is intermediate between those of the blocks heat-treated isothermally at 750 °C for 1 h and non-isothermally up to 900 °C.

It emerges that by judicious control of the firing cycle, it is possible to design the microstructure of these commercially available dental glass-ceramics from well-dispersed fine Li_2SiO_3 crystals embedded in an abundant glassy matrix to interlocked large $Li_2Si_2O_5$ crystals with little glassy phase in-between plus abundant surface CeO_2 crystals. According to the FE-SETM observations shown in Fig. 14, performed in-situ at 25, 750, 800, and 900 °C, there is little microstructural development at 750 °C but evident crystal lengthening at 900 °C, with the intermediate temperatures then promoting different degrees of microstructural coarsening. Also, CeO_2 precipitation is already inferred in the FE-SETM images taken at 800 °C, but becomes more noticeable in those taken at 900 °C. Given the ample repertoire of possible microstructures, further work is then needed to elucidate the effects of the microstructure on both the aesthetic aspects and mechanical/tribological properties of these glass-ceramics with a focus towards the optimization of their performance and lifespan as dental restorations. The conventional wisdom is that fine-grained microstructures maximize the strength and wear resistance of ceramics, while coarsened-microstructures (especially if elongated) maximize their toughness. Earlier studies [38,39] on lithium disilicate glass-ceramics suggest however that their ideal microstructures (in terms of strength, toughness, and wear resistance) are those formed by interlocked medium-sized $Li_2Si_2O_5$ grains, which best balance conflicting effects of grain size, residual stress, and crystallinity degree. Whether this processing guideline extends to commercially available dental-grade lithium disilicate glass-ceramics is nonetheless an important question with relevant clinical implications that remains to be resolved with further systematic studies.

4. Concluding remarks

The microstructural development during the heat treatment of a commercially available dental-grade glass-ceramic, which consisted essentially of small Li_2SiO_3 crystals embedded in a glassy matrix, was studied using a battery of in-situ and ex-situ characterization techniques. It was observed that the

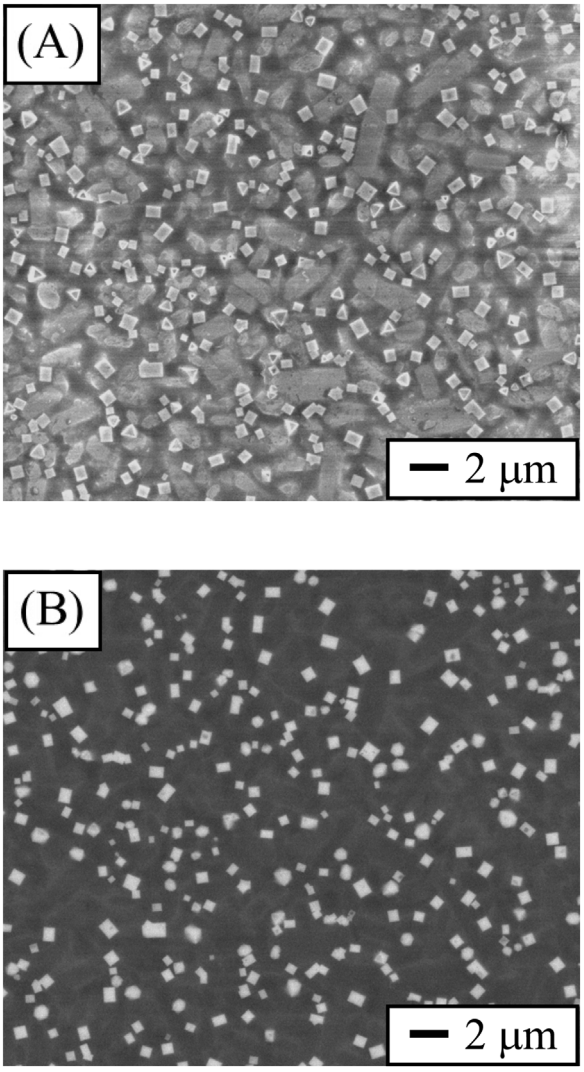

Fig. 13 – Representative SEM micrographs of the block resulting from the isothermal heating at 850 °C for 1 h, taken with the (A) LVSED and (B) BSED.

microstructure remains unchanged up to ~660 °C, at which temperature SiO_2 crystallizes (in the form of cristobalite) from the glass. With further temperature increase, the solid-state reaction $Li_2SiO_3 + SiO_2 \rightarrow Li_2Si_2O_5$ starts at ~735 °C and is completed at ~770 °C. Precipitation of colouring Ce ions, in the form of surface CeO_2, also occurs at ~775 °C. Finally, it was demonstrated that, by appropriate control of the heat treatment conditions, it is feasible to optimize the microstructure of these glass-ceramics for dental restorations from well-dispersed fine Li_2SiO_3 crystals embedded in an abundant glassy matrix to interlocked large $Li_2Si_2O_5$ crystals with less glassy phase in-between plus abundant surface CeO_2 crystals.

Acknowledgements

This work was supported by the Junta de Extremadura and FEDER Funds under Grant number IB16139, and the United States National Institutes of Health, National Institute of Dental and Craniofacial Research under Grant numbers R01DE026772 and R01DE026279. Financial support from the Ministerio de Economía y Competitividad (Government of Spain) and FEDER Funds under Grant number MAT2016-76638-R is gratefully acknowledged as well. Thanks are also due to Drs M. Carbajo, R. Pedrero, and D. Gamarra (at the SAIUEx) for the fruitful assistance provided.

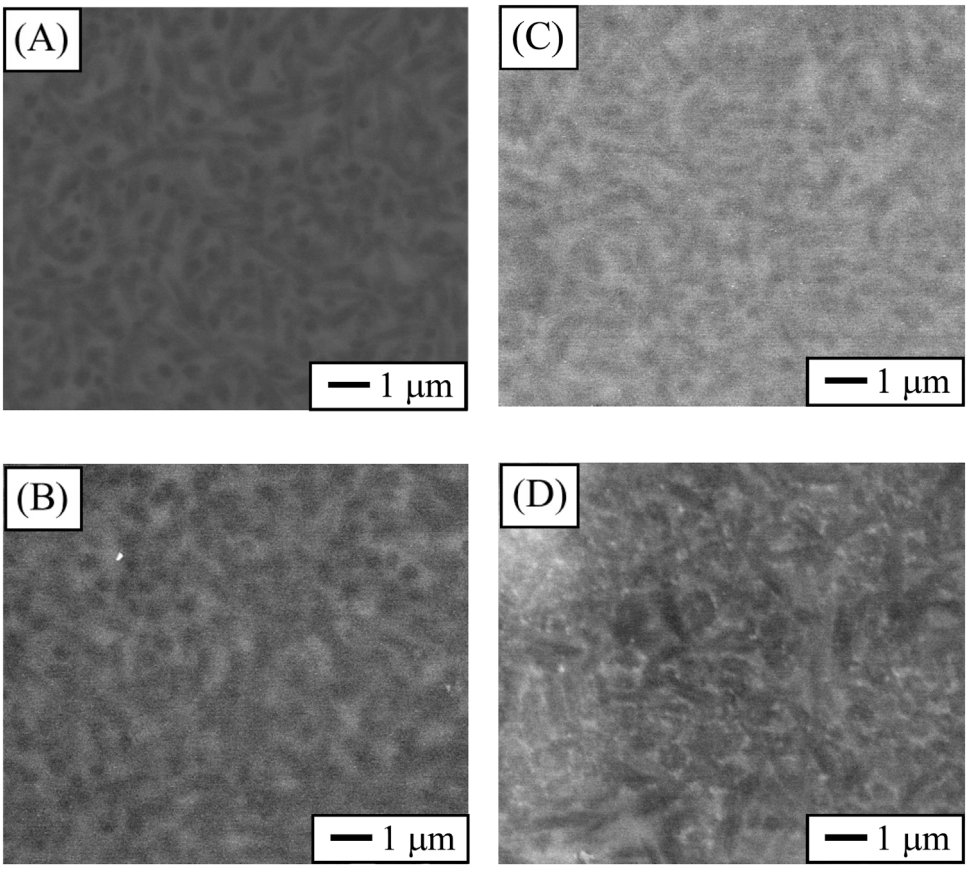

Fig. 14 – Representative SEM micrographs of the blue block taken in-situ with the GSED at (A) 25, (B) 750, (C) 800, and (D) 900 °C, after 5 min of holding time for temperature stabilization.

REFERENCES

[1] Tagtekin DA, Ozyoney G, Yanikoglu F. Two-year clinical evaluation of IPS Empress II ceramic onlays/inlays. Oper Dent 2009;34:369–78.

[2] Marquardt P, Strub JR. Survival rates of IPS Empress 2 all-ceramic crowns and fixed partial dentures: results of a 5-year prospective clinical study. Quintessence Int 2006;37:253–9.

[3] Taskonak B, Sertgöz A. Two-year clinical evaluation of lithia-disilicate-based all-ceramic crowns and fixed partial dentures. Dent Mater 2006;22:1008–13.

[4] Valenti M, Valenti A. Retrospective survival analysis of 261 lithium disilicate crowns in a private general practice. Quintessence Int 2009;40:573–9.

[5] Esquivel-Upshaw JF, Anusavice KJ, Young H, Jones J, Gibbs C. Clinical performance of a lithia disilicate-based core ceramic for three-unit posterior FPDs. Int J Prosthodont 2004;17:469–75.

[6] Makarouna M, Ullmann K, Lazarek K, Boening KW. Six-year clinical performance of lithium disilicate fixed partial dentures. Int J Prosthodont 2011;24:204–6.

[7] Alao AR, Stoll R, Song XF, Abbott JR, Zhang Y, Abduo J, et al. Fracture, roughness and phase transformation in CAD/CAM milling and subsequent surface treatments of lithium metasilicate/disilicate glass-ceramics. J Mech Behav Biomed Mater 2017;74:251–60.

[8] Apel E, Deubener J, Bernard A, Holand M, Muller R, Kappert H, et al. Phenomena and mechanisms of crack propagation in glass-ceramics. J Mech Behav Biomed Mater 2008;1:313–25.

[9] Holand W, Rheinberger V, Apel E, van't Hoen C, Holand M, Dommann A, et al. Clinical applications of glass-ceramics in dentistry. J Mater Sci Mater Med 2006;17:1037–42.

[10] Peng Z, Izzat Abdul Rahman M, Zhang Y, Yin L. Wear behavior of pressable lithium disilicate glass ceramic. J Biomed Mater Res B Appl Biomater 2016;104:968–78.

[11] Zhang Y, Kelly JR. Dental ceramics for restoration and metal veneering. Dent Clin North Am 2017;61:797–819.

[12] Wendler M, Belli R, Petschelt A, Mevec D, Harrer W, Lube T, et al. Chairside CAD/CAM materials. Part 2: flexural strength testing. Dent Mater 2017;33:99–109.

[13] Zhang Y, Lee JJ, Srikanth R, Lawn BR. Edge chipping and flexural resistance of monolithic ceramics. Dent Mater 2013;29:1201–8.

[14] Kern M, Sasse M, Wolfart S. Ten-year outcome of three-unit fixed dental prostheses made from monolithic lithium disilicate ceramic. J Am Dent Assoc 2012;143:234–40.

[15] Wolfart S, Eschbach S, Scherrer S, Kern M. Clinical outcome of three-unit lithium-disilicate glass-ceramic fixed dental prostheses: up to 8 years results. Dent Mater 2009;25:e63–71.

[16] Lien W, Roberts HW, Platt JA, Vandewalle KS, Hill TJ, Chu TM. Microstructural evolution and physical behavior of a lithium disilicate glass-ceramic. Dent Mater 2015;31:928–40.

[17] Guess PC, Vagkopoulou T, Zhang Y, Wolkewitz M, Strub JR. Marginal and internal fit of heat pressed versus CAD/CAM fabricated all-ceramic onlays after exposure to thermo-mechanical fatigue. J Dent 2014;42:199–209.

[18] Holand W, Apel E, van't Hoen C, Rheinberger V. Studies of crystal phase formations in high-strength lithium disilicate glass-ceramics. J Non-Cryst Solids 2006;352:4041–50.
[19] Holand W, Rheinberger V, Apel E, Ritzberger C, Eckert H, Monster C. Mechanisms of nucleation and crystallisation in high strength glass-ceramics. Phys Chem Glasses B 2007;48:97–102.
[20] Apel E, van't Hoen C, Rheinberger V, Höland W. Influence of ZrO_2 on the crystallization and properties of lithium disilicate glass-ceramics derived from a multi-component system. J Eur Ceram Soc 2007;27:1571–7.
[21] Burgner LL, Weinberg MC. An assessment of crystal growth behavior in lithium disilicate glass. J Non-Cryst Solids 2001;279:28–43.
[22] Hammetter W, Loehman R. Crystallization kinetics of a complex lithium silicate glass-ceramic. J Am Ceram Soc 1987;70:577–82.
[23] Huang S, Cao P, Li Y, Huang Z, Gao W. Nucleation and crystallization kinetics of a multicomponent lithium disilicate glass by in situ and real-time synchrotron X-ray diffraction. Cryst Growth Des 2013;13:4031–8.
[24] Soares PC, Zanotto ED, Fokin VM, Jain H. TEM and XRD study of early crystallization of lithium disilicate glasses. J Non-Cryst Solids 2003;331:217–27.
[25] Huang S, Cao P, Wang C, Huang Z, Gao W. Fabrication of a high-strength lithium disilicate glass-ceramic in a complex glass system. J Asian Ceram Soc 2013;1:46–52.
[26] Huang S, Li Y, Wei S, Huang Z, Gao W, Cao P. A novel high-strength lithium disilicate glass-ceramic featuring a highly intertwined microstructure. J Eur Ceram Soc 2017;37:1083–94.
[27] Höland W, Apel E, van't Hoen C, Rheinberger V. Studies of crystal phase formations in high-strength lithium disilicate glass–ceramics. J Non-Cryst Solids 2006;352:4041–50.
[28] Huang S, Huang Z, Gao W, Cao P. In situ high-temperature crystallographic evolution of a nonstoichiometric $Li_2O{\cdot}2SiO_2$ glass. Inorg Chem 2013;52:14188–95.
[29] Huang S, Huang Z, Gao W, Cao P. Structural response of lithium disilicate in glass crystallization. Cryst Growth Des 2014;14:5144–51.
[30] Huang S, Huang Z, Gao W, Cao P. Trace phase formation, crystallization kinetics and crystallographic evolution of a lithium disilicate glass probed by synchrotron XRD technique. Sci Rep 2015;5:9159.
[31] Based on global sales figures. Ivoclar Vivadent Corporate; 2018,. www.ivoclarvivadent.com/en/p/all/ips-emax-system-dentists/ips-emax-cad-chairside.
[32] Borlaf M, Colomer MT, Moreno R, Ortiz AL. Effect of Er^{3+} doping on the thermal stability of TiO_2 nanoparticulate xerogels. J Nanopart Res 2013;15:1752.
[33] Borlaf M, Colomer MT, Moreno R, Ortiz AL. Rare earth-doped TiO_2 nanocrystalline thin films: preparation and thermal stability. J Eur Ceram Soc 2014;34:4457–62.
[34] Colomer MT, Ortiz AL. Effect of Tb^{3+} doping and self-generated pressure on the crystallographic/morphological features and thermal stability of $LaPO_4{\cdot}nH_2O$ single-crystal nanorods obtained by microwave-assisted hydrothermal synthesis. Ceram Int 2016;42:18074–86.
[35] Colomer MT, Ortiz AL, López-Domínguez V, Alonso JM, García MA. Preparation, thermal and phase evolution and functional properties of non-stoichiometric strontium-doped lanthanum manganite perovskite ceramics. J Eur Ceram Soc 2017;37:527–3533.
[36] Colomer MT, Zur L, Ferrari M, Ortiz AL. Structural-microstructural characterization and optical properties of Eu^{3+},Tb^{3+}-codoped $LaPO_4{\cdot}nH_2O$ and $LaPO_4$ nanorods hydrothermally synthesized with microwaves. Ceram Int 2018;44:11993–2001.
[37] Monmaturapoj N, Lawita P, Thepsuwan W. Characterisation and properties of lithium disilicate glass ceramics in the SiO_2-Li_2O-K_2O-Al_2O_3 system for dental applications. Adv Mater Sci Eng 2013;2013:11p, 763838.
[38] Zhang Z, Guo J, Sun Y, Tian B, Zheng X, Zhou M, et al. Effects of crystal refining on wear behaviors and mechanical properties of lithium disilicate glass-ceramics. J Mech Behav Biomed Mater 2018;81:52–60.
[39] Hallmanna L, Ulmer P, Kern M. Effect of microstructure on the mechanical properties of lithium disilicate glass-ceramics. J Mech Behav Biomed Mater 2018;82:355–70.